The Journal of Chemical Physics

Theory of repulsive charged colloids in slit-pores

Cite as: J. Chem. Phys. **137**, 014702 (2012); https://doi.org/10.1063/1.4730923
Submitted: 10 February 2012 . Accepted: 08 June 2012 . Published Online: 03 July 2012

Alberto Gallardo, Stefan Grandner, Noé G. Almarza, and Sabine H. L. Klapp

Theory of repulsive charged colloids in slit-pores

Alberto Gallardo,[1,a)] Stefan Grandner,[2] Noé G. Almarza,[1] and Sabine H. L. Klapp[2]
[1]*Instituto de Química-Física Rocasolano, CSIC, Serrano 119, E-28006 Madrid, Spain*
[2]*Institut für Theoretische Physik, Technische Universität Berlin, Hardenbergstrasse 36, D-10623 Berlin, Germany*

(Received 10 February 2012; accepted 8 June 2012; published online 3 July 2012)

Using classical density functional theory (DFT) we analyze the structure of the density profiles and solvation pressures of negatively charged colloids confined in slit pores. The considered model, which was already successfully employed to study a real colloidal (silica) suspension [S. H. L. Klapp *et al.*, Phys. Rev. Lett. **100**, 118303 (2008)], involves only the macroions which interact via the effective Derjaguin-Landau-Verwey-Overbeek (DLVO) potential supplemented by a hard core interaction. The solvent enters implicitly via the screening length of the DLVO interaction. The free energy functional describing the colloidal suspension consists of a hard sphere contribution obtained from fundamental measure theory and a long range contribution which is treated using two types of approximations. One of them is the mean field approximation (MFA) and the remaining is based on Rosenfeld's perturbative method for constructing the Helmholtz energy functional. These theoretical calculations are carried out at different bulk densities and wall separations to compare finally to grand canonical Monte Carlo simulations. We also consider the impact of charged walls. Our results show that the perturbative DFT method yields generally qualitatively consistent and, for some systems, also quantitatively reliable results. In MFA, on the other hand, the neglect of charge-induced correlations leads to a breakdown of this approach in a broad range of densities. © *2012 American Institute of Physics*. [http://dx.doi.org/10.1063/1.4730923]

I. INTRODUCTION

The study of colloidal suspensions subject to spatial confinement is an active field of research with many interesting technological applications in lubrication, adhesion, and design of nanomaterials. Moreover, these type of systems are very interesting from a theoretical point of view, because their study makes possible to understand the physics that occurs due to finite-size effects, surface forces, and reduced dimensionality. The spatial confinement can induce significant changes of the structure and phase behavior of a fluid as compared to its bulk properties. In the case of a fluid inside of a slit pore the translational symmetry of the bulk system is broken in one spatial direction. This causes the colloid particles to form layers parallel to the walls.

In the present work, we employ density functional theory (DFT) and grand canonical Monte Carlo (GCMC) simulations to study a colloidal suspension of (negatively) charged particles with moderate Coulomb coupling confined between two plane-parallel charged surfaces. The model, including our choice of parameters, is inspired by a real colloidal suspension consisting of silica particles.[1] We perform DFT calculations, using fundamental measure theory (FMT) to treat the hard core interaction. The FMT (Refs. 2 and 3) is known to give excellent results for pure hard sphere systems. The long range repulsion is treated considering two kinds of approximations. One of them is the mean field approximation (MFA), where the excess free energy functional can be obtained from a perturbative expansion to lowest order of the pair potential.[4] The other approximation is a perturbative method suggested by Rosenfeld in the spirit of the mean spherical approximation.[5]

Most previous DFT studies involving colloidal suspensions are focused on a hard-sphere like interaction between the colloidal particles, with a special emphasis on the Asakura-Oosawa model, additive and nonadditive hard sphere mixtures.[6–8] On the other hand, there are previous works which consider long range interactions but they are focused on potentials with an attractive tail, as typically represented by the Lennard-Jones (LJ) potential. Even to date, MFA is the most popular method used in DFT calculations, because this approximation is computationally efficient and can describe some inhomogeneous phenomena.[9] Nevertheless, it is known that its performance is highly system-dependent and can yield wrong results due to the fact that MFA neglects the fluid structure completely. There have been earlier efforts to find non-mean-field approaches, which take into account correlations between the particles. One of these approaches is the above-mentioned method proposed by Rosenfeld, which provides an expression for the long range contribution to free energy functional, taking as reference the uniform system. Earlier works have used this method together with a first-order mean spherical approximation (FMSA) to study Lennard-Jones fluids[10] and Yukawa fluids[11] obtaining satisfactory results.

An important aspect we must take into account is that most intercolloidal interactions considered by theoretical models are effective models in the sense that some microscopic degrees of freedom are averaged out. These mean or effective forces are an important key to understand the structure and stability of the colloidal suspension. In this work,

a)Electronic mail: a.gallardo@iqfr.csic.es.

we study a charged colloidal suspension involving (negatively charged) macroions. The effective interaction between these macroions is modeled by Derjaguin-Landau-Verwey-Overbeek (DLVO) potential that is essentially a repulsive Yukawa-like potential. The surrounding (monovalent) counterions and salt ions, which constitute the solvent phase, are implicitly treated.

Our goal is to investigate the density profiles and solvation pressure using DFT methods combined with the aforementioned MFA and FMSA. This allows us to systematically test the theoretical approximations comparing their predictions to GCMC simulation results.

The remainder of this paper is arranged as follows. In Sec. II we briefly describe the model, giving a detailed information about the fluid-fluid and the fluid-wall interaction potentials. The density functional theory formalism including information about the free energy functionals expressions are presented in the Sec. III A. Details of Monte Carlo simulations are described in Sec. III B. Our DFT results for a system with uncharged walls are presented in Sec. IV A, where we also compare to MC results. In Sec. IV B, we present our DFT and GCMC results for systems with charged walls. Finally, Sec. V is devoted to concluding remarks.

II. MODEL

The colloidal suspension considered in this work consists of macroions, counterions, salt ions, and solvent molecules. The macroions are negatively charged particles, and the Coulomb interaction between them is screened exponentially by the surrounding counterions and salt ions. Following earlier works,[1,12–15] we model the bulk colloidal solution on an effective level via the electrostatic part of the DLVO potential.[4,16] The latter involves only the macroions and the rest of components are treated implicitly in the model. Therefore, the corresponding macroion-macroion interaction takes the form of a Yukawa repulsion,

$$u_{DLVO}(r) = W\frac{\exp(-\kappa r)}{r}, \tag{1}$$

where r is the distance between the centers of two macroions and the prefactor W is

$$W = \frac{(\widetilde{Z}e_0)^2}{4\pi\epsilon_0\epsilon}\exp(\kappa\sigma). \tag{2}$$

In Eq. (2), ϵ_0 and ϵ are the permittivity of the vacuum and the relative permittivity of the solvent, respectively. The parameter e_0 is the elementary charge, σ is the macroion diameter. Further, $\widetilde{Z} = Z/(1+\kappa\sigma/2)$ is an effective valency, where κ is the inverse Debye screening length, which is defined as

$$\kappa = \sqrt{\frac{e_0^2}{\epsilon_0\epsilon k_B T}(Z\rho_b + 2IN_A)}, \tag{3}$$

where ρ_b is the macroions bulk density, N_A is the Avogadro's constant, and the ionic strength I is a measure of the salt concentration. By means of κ our model takes into account the dependence of the effective macroion interaction on the temperature T and the macroion density.

In order to model the steric repulsion, we use different approaches in the GCMC simulations and the DFT calculations. Specifically, in the simulations we use the repulsive part of a Lennard-Jones potential, $u_{SS}(r) = 4\,\epsilon_{SS}(\sigma/r)^{12}$ (the LJ parameter is set to $\epsilon_{SS}/k_BT = 1$). In the case of density functional calculations, we have supplemented the DLVO potential by a hard sphere (HS) interaction. We have chosen a different potential because the HS interaction is a more convenient starting point for approximations within the DFT. In practice, however, the differences between the two models are negligible since the diameter of the soft-sphere described with u_{SS} is practically equal to its corresponding effective Barker-Henderson diameter[17,18] $\sigma_{BH} \simeq \sigma$ (at the LJ parameter considered in this work). We will briefly come back to the role of the actual shape of the repulsion at the beginning of the Sec. IV. The total fluid-fluid (FF) interaction for each sort of calculation is

$$u_{FF}^{SIMU}(r) = u_{DLVO}(r) + u_{SS}(r), \tag{4}$$

in the MC simulations and

$$u_{FF}^{DFT}(r) = u_{DLVO}(r) + u_{HS}(r) = \begin{cases}\infty & r < \sigma \\ u_{DLVO}(r) & r \geq \sigma,\end{cases} \tag{5}$$

in the DFT calculations. In Eq. (5), $u_{HS}(r)$ is the HS potential. The DLVO parameters are chosen according to the colloidal-probe atomic force microscope (CP-AFM) experiments described in Refs. 1 and 15. These experiments involve suspensions of Ludox silica particles with a diameter $\sigma = 26\,\text{nm}$ and charge $Z = 35$. Furthermore, the suspensions are characterized by the temperature $T = 298\,K$, dielectric constant $\epsilon = 78.5$, and ionic strength $I = 10\,\text{mol/l}$.

We consider the colloidal solution to be confined between two plane-parallel walls at positions $z = 0$ and $z = L_z$. The confining potential is given by the integrated soft-wall (SW) potential[4]

$$u_{FS}^{SW}(z) = \frac{4}{45}\pi\epsilon_w\left(\frac{\sigma}{z}\right)^9, \tag{6}$$

where we set $\epsilon_w/k_BT = 1$. In Eq. (6), z is the distance of the center of the fluid particle from the wall at position $z = 0$. In addition, we have investigated the impact of charged walls.[14] The latter are modeled by a modified version of the linearized Poisson-Boltzmann (PB) theory using linear superposition approximation (LSA) and Derjaguin approximation.[19] The resulting screening parameter depends on the distance of the macroions from the wall and the wall charge. The corresponding interaction potential between a macroion and a charged wall reads

$$u_{FS}^{LSA} = 64\pi\epsilon_0\epsilon\gamma_F\gamma_S\frac{\sigma}{2}\left(\frac{k_BT}{e_0}\right)^2\exp\left[-\kappa_W(z)\left(z-\frac{\sigma}{2}\right)\right], \tag{7}$$

where $\gamma_{F/S} = \tanh(e_0\psi_{F/S}/4k_BT)$, and $\psi_{F/S}$ is the surface potential of the fluid particles (F) and the solid walls (S). The present calculations involve silica macroions which are characterized by a surface potential of $\psi_F = -80\,\text{mV}$. The expression for the screening parameter $\kappa_W(z)$ is given by

$$\kappa_W(z) = \sqrt{\frac{e_0^2}{\epsilon_0\epsilon k_BT}\left(Z\rho_b + 2IN_A + \frac{|\sigma_s|}{e_0 z}\right)}. \tag{8}$$

In Eq. (8), σ_s is the surface charge density. The latter is related to the surface potential via the Grahame equation[20] $\sigma_s = \sqrt{8c_0\epsilon_0\epsilon k_B T}\,\sinh(e_0\psi_S/2k_BT)$, where c_0 is the total ion concentration of the bulk suspension; more detailed information about potential parameters and their values are given in the Ref. 14 . Finally, the total fluid-solid interaction is given by

$$u_{FS}(z) = u^w_{FS}(z) + u^w_{FS}(L_z - z) = u^{SW}_{FS}(z) + u^{LSA}_{FS}(z) + u^{SW}_{FS}(L_z - z) + u^{LSA}_{FS}(L_z - z), \tag{9}$$

where L_z is the distance between the walls. We have implicitly assumed that the single-wall potentials from the two charged walls are additive.

III. METHODS

A. Density functional theory

Classical DFT is now well-established as the most successful theory to study the equilibrium structure and thermodynamics of inhomogeneous fluids. The natural ensemble to study confined systems as those considered in the present work is the grand canonical ensemble. The corresponding thermodynamic potential, the grand potential, can be considered as a functional of the one-body profile $\rho(\mathbf{r})$. Its expression is

$$\Omega[\rho(\mathbf{r})] = F[\rho(\mathbf{r})] + \int d^3r\, \rho(\mathbf{r})(V_{ex}(\mathbf{r}) - \mu), \tag{10}$$

where μ and $V_{ex}(\mathbf{r})$ are the chemical and the external potential, respectively. The functional of the intrinsic Helmholtz free energy $F[\rho(\mathbf{r})]$ can be split into ideal, hard sphere, and DLVO contributions,

$$F[\rho(\mathbf{r})] = F_{id}[\rho(\mathbf{r})] + F_{HS}[\rho(\mathbf{r})] + F_{DLVO}[\rho(\mathbf{r})], \tag{11}$$

where the ideal part F_{id} is

$$F_{id}[\rho(\mathbf{r})] = \beta^{-1}\int d^3r\ \rho(\mathbf{r})\big[ln\big(\rho(\mathbf{r})\Lambda_s^3\big) - 1\big], \tag{12}$$

and Λ_s is a particle length scale. We treat the HS contribution via FMT, yielding

$$F_{HS}[\rho(\mathbf{r})] = \beta^{-1}\int d^3r\, \Phi^{WB}(n_\alpha, \mathbf{n}_\beta), \tag{13}$$

where $\Phi^{WB}(n_\alpha, \mathbf{n}_\beta)$ is the "White Bear" version[3,21] for the expression of the free energy density. This free energy density is a function of a set of scalar and vectorial weighted density functions, which are given by

$$n_\alpha(\mathbf{r}) = \int d^3r'\, \rho(\mathbf{r}')\,\omega_\alpha(\mathbf{r} - \mathbf{r}'),$$
$$\mathbf{n}_\beta(\mathbf{r}) = \int d^3r'\, \rho(\mathbf{r}')\vec{\omega}_\beta(\mathbf{r} - \mathbf{r}'). \tag{14}$$

The weighted functions $\{\omega_\alpha\}$ and $\{\vec{\omega}_\beta\}$ are defined in terms of Dirac-delta distributions $\delta(r)$ and Heaviside step functions $\Theta(r)$. Explicit expressions for the weight functions are given in Refs. 2 and 3.

To obtain the functional expressions associated with the DLVO interaction, we have used two types of approximations, MFA (Ref. 4) and a perturbative method proposed by Rosenfeld.[5] The corresponding intrinsic free energy functional for the DLVO interaction with MFA reads

$$F^{MF}_{DLVO}[\rho(\mathbf{r})] = \frac{1}{2}\beta^{-1}\int d^3r \int d^3r'\rho(\mathbf{r})\,u_{DLVO}(|\mathbf{r} - \mathbf{r}'|)\rho(\mathbf{r}'). \tag{15}$$

In Eq. (15), we observe that MFA ignores entirely correlations induced by the DLVO interaction. The second theoretical approximation is constructed by a perturbation expansion of the free energy of the inhomogeneous system around the bulk fluid,

$$F^{FMSA}_{DLVO}[\rho(\mathbf{r})] = F_{DLVO}(\rho_b) + \mu_{DLVO}\int d^3r'\Delta\rho(\mathbf{r}') - \frac{1}{2}\beta^{-1}\int d^3r' \int d^3r'' c_{DLVO}(\mathbf{r}' - \mathbf{r}'')\Delta\rho(\mathbf{r}')\Delta\rho(\mathbf{r}''), \tag{16}$$

where $\Delta\rho(\mathbf{r}) = \rho(\mathbf{r}) - \rho_b$, ρ_b is the bulk density and μ_{DLVO} is the DLVO part of the excess chemical potential. The function $c_{DLVO}(\mathbf{r})$ is the direct correlation function (DCF) of the bulk fluid, which is a key input into the perturbation approach. In the present work, we have calculated the DCF via the FMSA.[22] The latter is a modification of the well-known MSA, which has been widely used to calculate correlation functions of model fluids whose pair potential consists of a HS interaction plus a tail. An attractive feature of the MSA is that it provides analytical expressions for the DCF for a wide range of models, including Yukawa-like potentials.[23] However, to actually use these expressions one needs to obtain several parameters numerically from a set of nonlinear equations. Another complication related to the MSA is the appearance of regions in the parameter space where no solutions exist.[22,24] This problem is overcome within the FMSA suggested by Tang.[10] Indeed, the FMSA provides an entirely analytical expression for DCF, that is, all the parameters can be obtained directly. This makes the implementation of FMSA within our DFT calculations as easy and efficient as those based on the mean field approach.[10]

The equilibrium density profiles are determined by the fundamental variational principle of DFT.[25] Applied to classical systems[26] this principle state that the total grand potential $\Omega[\rho]$ [see Eq. (10)] is minimal with respect to variations of the density profile,

$$\left[\frac{\delta\Omega[\rho(\mathbf{r})]}{\delta\rho(\mathbf{r})}\right]_{\rho(\mathbf{r})=\rho_0(\mathbf{r})} = 0, \tag{17}$$

where ρ_0 is the equilibrium density profile.[26] Once the equilibrium density profile has been determined we can calculate the normal pressure P_{zz} as a function of the wall separation. Using the functional relation[27] and the symmetry properties of u_{FS} and $\rho(z)$, P_{zz} can be expressed as

$$P_{zz} = -\int_{-\infty}^{\infty} dz\,\rho(z)\,\frac{du^w_{FS}}{dz}, \tag{18}$$

where u_{FS}^{w} is the total interaction potential of a single wall, consist of the soft potential $u_{FS}^{SW}(z)$ and charged wall potential $u_{FS}^{LSA}(z)$. Another useful quantity is the solvation pressure $f(L_z)$, which is defined as

$$f(L_z) = P_{zz}(L_z) - P_b. \tag{19}$$

Here, P_b is the pressure of the bulk system at the same chemical potential as the inhomogeneous system, and $P_{zz}(L_z)$ is the normal pressure for a fixed distance between the walls. An important feature of the solvation pressure is that it is accessible not only by theory and simulations, but also by (e.g., CP-AFM) experiments (see, e.g., Ref. 15). Moreover, by analyzing the behavior of $f(L_z)$ for large L_z (i.e., in the asymptotic regime), one can obtain valuable information about the fluid structure[1,6] (see also Sec. IV B). In the present study, we have obtained the bulk pressure P_b appearing in Eq. (19) by taking the limit $L_z \to \infty$ of the function $P_{zz}(L_z)$, i.e., by searching for those wall separations where the oscillations in $P_{zz}(L_z)$ disappear. In practice, this is the case if L_z becomes lager than 10–15 particle diameters (depending of the bulk density considered). Additionally, we have performed some test calculations where we determined the bulk pressure via the contact theorem, i.e., via the density profile at the wall. The results turned out to be consistent with those from $P_{zz} \to \infty$.

B. Computer simulations

The confined colloidal suspension is in contact with a reservoir at fixed chemical potential μ and temperature T. Therefore, we have first carried out canonical (N, V, T) bulk simulations in combination with the Widom particle insertion method[28] to obtain the chemical potential μ. Afterwards, the calculated values of μ are then used as an input for the GCMC simulations.[29] Each GCMC simulation is carried out at fixed temperature T, chemical potential μ, wall separation L_z, and area parallel to the walls A. For bulk simulations we employ a cubic simulation cell with periodic boundary conditions in all three spatial directions. In the case of GCMC simulations, the simulation box is a cuboid, where L_z generally differs from lengths in the plane parallel to the walls. Periodic conditions are only applied in the directions x and y. The simulations were carried out with about $N = 500$ particles, but the particle number was occasionally extended to up to 2000 particles to reduce the system size effects particularly for the strongly confined systems. On average, we performed on the order of $(15 - 25) \times 10^3$ steps of equilibration per particle followed by a production period of about the same length. Further technical details about simulations can be found in Ref. 13. The aim of the GCMC simulations is to obtain the density profiles and the effective forces induced by the particles on the walls. This effective force per unit area is the normal pressure P_{zz}, which can be determined from the virial expression[30]

$$P_{zz} = k_B T \left\langle \frac{N}{L_z A} \right\rangle - \left\langle \frac{1}{A} \frac{\partial U_T}{\partial L_z} \right\rangle. \tag{20}$$

The first term is the ideal pressure contribution and the last term is a derivative of the total potential energy U_T with respect to the distance between the walls. This potential U_T is the interaction energy involving both fluid-fluid and fluid-wall contributions. In the present work, the normal pressures, solvation pressure, and densities are presented in the reduced form $P_{zz}^* = P_{zz}\sigma^3/k_BT$, $f^* = f\sigma^3/k_BT$, and $\rho^* = \rho\sigma^3$, respectively.

IV. RESULTS

A. System with uncharged walls

In the following, we present results of our DFT calculations and compare these to the GCMC simulation results. We consider first the simplest model for the fluid-wall interaction, that is, the case of uncharged walls [see Eq. (6)]. Since the most direct output of the DFT are the density profiles, we start by considering these quantities.

However, before going into the actual comparison between DFT and GCMC, we briefly recall that the short-range repulsive part of the pair potential is different in the two methods [see Eqs. (4) and (5)]. To better evaluate the importance of this point, we have performed several GCMC simulations involving hard-spheres plus DLVO interactions (as in the DFT), on one hand, and soft-sphere plus DLVO interactions, on the other hand. With both models, we have obtained density profiles for strongly confined systems ($L_z^* = L_z/\sigma = 2.9$) characterized by two different bulk densities. Results are shown in Fig. 1. Inspecting the data in Fig. 1 we conclude that there are

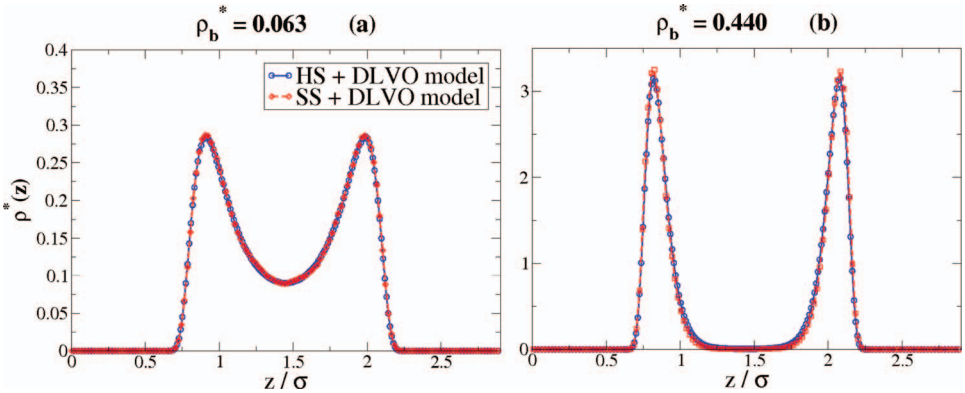

FIG. 1. GCMC density profiles for a system with walls separation $L_z^* = 2.9$ and uncharged walls. Their corresponding bulk densities are (a) $\rho_b^* = 0.063$, and (b) $\rho_b^* = 0.440$.

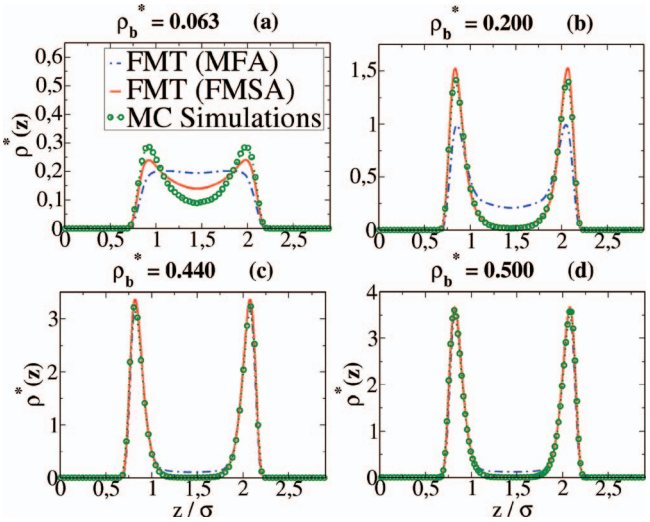

FIG. 2. Density profiles for a slit pore with a separation $L_z^* = 2.9$ and uncharged walls; (a) $\rho_b^* = 0.063$, (b) $\rho_b^* = 0.200$, (c) $\rho_b^* = 0.440$, and (d) $\rho_b^* = 0.500$.

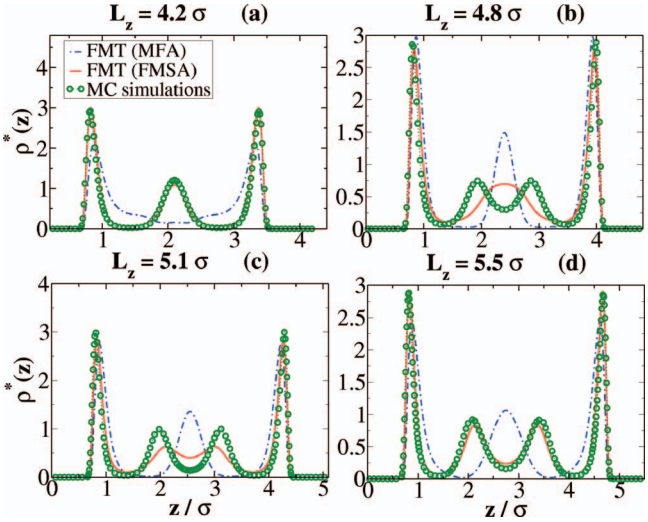

FIG. 3. Density profiles for systems with a bulk density $\rho_b^* = 0.440$ and uncharged walls; (a) $L_z^* = 4.2$, (b) $L_z^* = 4.8$, (c) $L_z^* = 5.1$, and (d) $L_z^* = 5.5$.

no appreciable difference; i.e., hard- and soft-sphere repulsion yield essentially the same profiles at parameters considered.

Keeping this in mind, we now focus on the DFT results. In the Fig. 2, we show exemplary density profiles obtained from the two DFT versions (FMSA and MFA) and GCMC simulations. The results pertain to a fixed wall separation of $L_z^* = 2.9$ and different bulk densities ρ_b^*. At the lowest density $\rho_b^* = 0.063$ [see Fig. 2(a)], the FMSA predicts correctly the existence of two layers, but underestimates the heights of the peaks as compared to the GCMC data. The MFA, on the other hand, is entirely wrong in the sense that predicts only one layer. As we consider higher bulk densities the agreement between DFT and simulation results improves. In fact, as shown in Fig. 2(b), already at $\rho_b^* = 0.200$ the FMSA yields good results and the MFA becomes at least qualitatively right. Finally, in Figs. 2(c) and 2(d), we observe that the agreement between FMSA and simulation is very good. At these higher bulk densities, the MFA also provides satisfactory results for the height of the peaks, but it exaggerates the density of particles between the two layers. Before carrying on with the discussion of the results, it is worth remembering that the value of the screening parameter κ depends on ρ_b^* [see Eq. (3)]. Therefore, each density pertains to a different fluid-fluid interaction, with the range of this interaction (determined by the inverse of κ) decreasing with increasing ρ_b^*. For that reason, a comparison of results with different densities cannot be done directly. This issue becomes particularly important when we aim to compare the performance of different DFT approximations.

We next consider density profiles for different wall separations L_z^* at a fixed, relatively high value of the bulk density. Some examples (for the case $\rho_b^* = 0.440$) are shown in Fig. 3. Inspecting these results, it becomes clear that the performance of our DFT approaches depends not only on the bulk density (as it is suggested by Fig. 2), but also on the actual value of the wall separation. More specifically, as shown in Figs. 3(a) and 3(b), the FMSA yields satisfactory results at $L_z^* = 4.2$, but not at $L_z^* = 4.8$. In the latter case, the GCMC predicts the formation of four layers of particles, where the the FMSA predicts only three. At $L_z^* = 5.1$, the FMSA profile describes (correctly) four layers, but the amplitude and position of the oscillations still deviates from the corresponding GCMC result. Finally, at $L_z^* = 5.5$ [see Fig. 3(d)] we observe very good agreement with the simulation data, similar to the case $L_z^* = 4.2$. Taken altogether, the FMSA is characterized by a "delay" (as compared to the GCMC) in predicting a new layer upon an increase of the wall separation (at fixed ρ_b^*). In the case of the MFA, this delay is even much larger; therefore this latter approximation provides consistently unsatisfactory results (that is, wrong number of layers) at the high density considered in Fig. 3. Clearly, in both the case of the FMSA and the FMA, any failures must be due to our treatment of the electrostatic correction to the excess free energy functional. We will come back to this point below.

Besides the density profiles themselves, additional information about the interplay of bulk density and wall separation in the context of our DFT approximations is given by the normal pressure P_{zz} as function of the wall separation. We have calculated this quantity at different bulk densities ρ_b^*. Results are given in Figs. 4 and 5.

An important piece of information is the corresponding value of the bulk pressure P_b^* (for the calculation of this

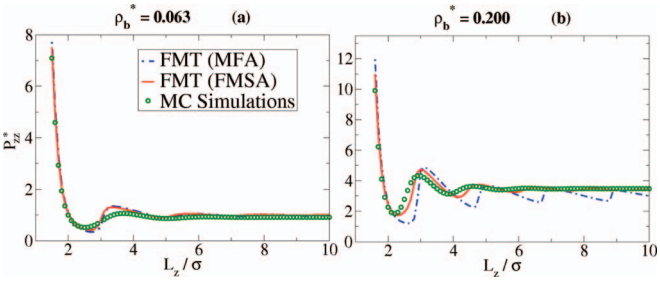

FIG. 4. Reduced normal pressure P_{zz}^* as function of wall separation L_z^*. The corresponding bulk densities are (a) $\rho_b^* = 0.063$ and (b) $\rho_b^* = 0.200$.

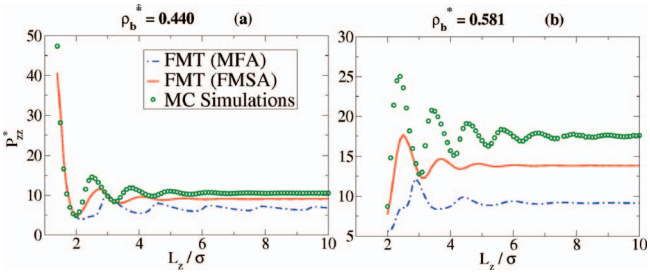

FIG. 5. Reduced normal pressure P^*_{zz} as function of wall separation L^*_z. Their corresponding bulk densities are (a) $\rho^*_b = 0.440$ and (b) $\rho^*_b = 0.581$.

quantity, see Eq. (19) below). This pressure is the asymptotic value of the function $P^*_{zz}(L^*_z)$ when the wall separation L^*_z tends to infinity. In Fig. 4(a) we show the normal pressure for a bulk density $\rho^*_b = 0.063$. At this density, both MFA and FMSA provide quite accurate (only slightly overestimated) values of the bulk pressure. This is seen from the fact that the two theoretical curves for large L^*_z a constant value, which is only slightly higher than the corresponding GCMC value. At finite values of L^*_z, the DFT results tend to exaggerate the oscillations, especially in the first minimum and maximum of $P^*_{zz}(L^*_z)$. Nevertheless, both approximations can be considered satisfactory. Figure 4(b) represents results for a system with a bulk density $\rho^*_b = 0.200$. In this case, both DFT approaches predict lower values of P^*_b. Moreover, the MFA yields a very slow decay of oscillations, and only the values close to the maxima of the function $P^*_{zz}(L^*_z)$ are in the vicinity of the GCMC results. The FMSA, on the other hand, reproduces satisfactorily the oscillations, with a slightly overestimation particularly at short wall distances.

Upon increasing the bulk density the DFT predictions for the bulk pressure worsen. These difficulties in describing more concentrated systems also concern the full function $P^*_{zz}(L^*_z)$, which displays pronounced oscillations according to GCMC results. This is illustrated in Figs. 5(a) and 5(b) where we find that the DFT predicts generally too weak (and shifted) oscillations. Still, the FMSA provides bulk pressure values nearer to simulation data as well as predicts at least a decay trend similar to the GCMC results. Moreover, the GCMC and FMSA data coincide exactly in some points located near the relative minima of P^*_z at small L^*_z. These coincidences correspond obviously to cases in which the FMSA yields particularly accurate density profiles. This is exactly what we observed in Figs. 2(c), 2(d), and 3(a): The density profiles shown there pertain to a wall separation $L^*_z = 2.9$. The latter value is localized near the second relative minimum of the oscillatory pressure curve [see Figs. 5(a) and 5(b)].

To better understand these findings we note that in both, GCMC and DFT approaches, a minimum in the normal pressure announces the formation of a new layer in the density profiles. This can be seen, for instance, by comparing the density profiles in Fig. 3 (where $\rho^*_b = 0.440$) with corresponding curve $P_{zz}(L_z)$ in Fig. 5. Focusing on the FMSA results we see that, at $L^*_z = 4.2$ [see Fig. 3(a)], the system consists of three layers, while the corresponding normal pressure is located between the second relative maximum and the third relative minimum of the function $P_{zz}(L_z)$. At $L^*_z = 4.8$, where the (FMSA) pressure is in a minimum, the central peak has become much wider and softer. Upon further increase of the separations, the normal pressure increases again, and the density profile now reflects four layers of particles [see Figs. 3(c) and 3(d)]. The same trends are seen in the quasi-exact GCMC results, with the appearance of the new layer happening at somewhat lower wall separation. As a consequence of the relative "delay" of the FMSA, all the minima are shifted towards somewhat larger values of L^*_z (compared to the GCMC). For example, at $\rho^*_b = 0.440$ [see Fig. 5(a)] the second relative minimum of P^*_{zz} is located at $L^*_z = 3.2$ within GCMC, while the FMSA and MFA second relative minima are located at $L^*_z = 3.4$ and $L^*_z = 4.0$, respectively.

Another interesting point apparent from Fig. 5 is that, at high bulk densities, the shifts of the FMSA normal pressure relative to the GCMC curve are most pronounced for large values of the wall separation. In other words, at small wall separations, where the system is dominated by the fluid-wall interactions the pressure oscillations are better described within the FMSA than at large wall separations, where the system becomes more and more bulk-like. In fact, as it is known from other studies,[6,31] the asymptotic decay of the pressure oscillations [see also Eq. (21)], particularly their wavelength and decay length, is governed by the bulk pair correlation function. In the present system, the interactions involve both a hard-core part (treated within the quasi-exact FMT) and an electrostatic part, which we treat in a perturbative fashion, i.e., by using some ansatz for the direct correlation function of the homogeneous system [see Eq. (16)]. Having this in mind, the deviations at larger wall separations can be understood as a hint to a corresponding failure of the FMSA approximation in predicting the correct bulk structure at high densities. A further hint is this direction is the fact, that also the pressure at large wall separations, that is, the bulk pressure predicted by FMSA, differs from the corresponding GCMC result. Of course, this is even more the case for the simpler MFA. Moreover, within the MFA, there is a large shift (relative to the GCMC data) of the curve $P^*_{zz}(L_z)$ in the entire range of wall separations.

Finally, apart from the shifts in the location of the minima and maxima, we note from Fig. 5, that the FMSA (and even more the MFA) is not capable of obtaining normal pressure values as high as the GCMC results. This is, to some extent, also reflected by the density profiles. As an illustration we present in Fig. 6 results for density profiles at wall separations close to the first or second maximum of the normal pressure. The first maximum [see Figs. 6(a) and 6(c)] corresponds to two-layer systems in both, DFT and MC calculations. However, we see that the DFT significantly underestimates the height of the peaks. Further, at wall separations related to the next maximum [see Figs. 6(b) and 6(d)], it is the central peak in the middle of the pore which is much too small within the DFT predictions. We conclude that the FMSA generally has difficulties in describing "sharp" density profiles corresponding to pressure maxima, but performs better when the profiles are softer (as it is typical at separations related to pressure minima).

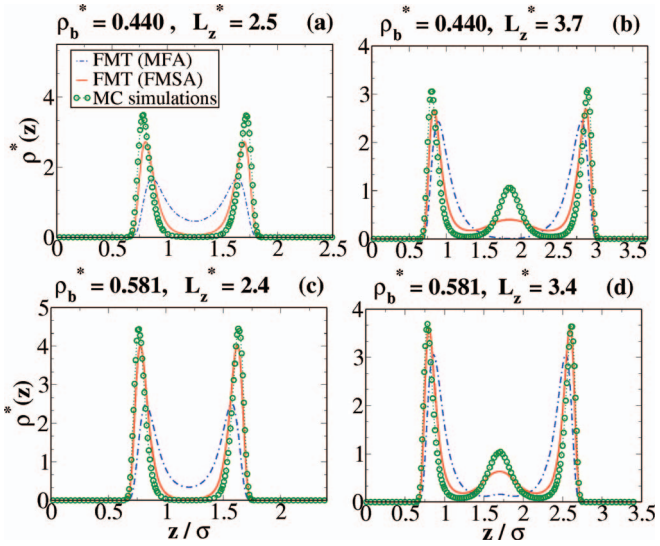

FIG. 6. Density profiles of systems whose normal pressure is located in the two first relative maxima. (a) $\rho_b^* = 0.440$ and $L_z^* = 2.5$; (b) $\rho_b^* = 0.440$ and $L_z^* = 3.7$; (c) $\rho_b^* = 0.581$ and $L_z^* = 2.4$; (d) $\rho_b^* = 0.581$ and $L_z^* = 3.4$.

Summarizing this section, we have seen that both DFT approximations give quite satisfactory results for low bulk densities. At higher densities, the MFA yields largely unsatisfactory results, presumably due to the fact that the corresponding free energy functional entirely neglects correlational effects beyond those of the HS interaction. The FMSA is generally more accurate in that it predicts in most cases correctly the number of layers and the general trend of the oscillatory pressure curves. Still, it has to be used with some caution. One feature seems to be a "delay" in the formation of new layers upon increase of L_z^*. The resulting errors seem to be the more pronounced, at the larger wall separations. Moreover, as shown by our calculations, the FMSA is not capable of providing sharp density profiles, which are characteristic of systems with normal pressures related to maxima in the function $P_{zz}(L_z)$.

B. System with charged walls

We now consider systems confined between charged surfaces. As described in Sec. II, we model this situation with a fluid-wall potential stemming from linearized PB theory, but with a space-dependent screening parameter [see Eqs. (7) and (8)]. This ansatz takes into account the fact that the charged walls release additional (wall) counterions which accumulate in a thin layer at the surfaces. In analogy to the colloidal-probe experiments and previous simulations described in Ref. 14, we set the surface potential of the (negatively charged) colloidal particles to $\psi_F = -80$ mV, whereas the surface potential of the (likewise negatively charged) walls varies between -160 mV $< \psi_S < 0$ mV. This range seems realistic in view of the actual surface materials used in the experiments, that silica surfaces ($\psi_S \approx -80$ mV), and mica surfaces ($\psi_S \approx -160$ mV). From an experimental point of view, a particularly interesting question related to modifications of the surfaces is the impact of such modifications on the oscillations of the solvation pressure, $f(L_z) = P_{zz} - P_b$ [see Eq. (19)].

As seen from Figs. 4 and 5 such oscillations (of the normal pressure and thus, the solvation pressure) occur already for the case of uncharged walls. In the asymptotic regime (that is, for large values of L_z), the oscillations are typically fitted according to the expression

$$f(L_z) \to A_f \exp(-L_z/\xi_f) \cos\left(\frac{2\pi}{\lambda_f} L_z - \theta_f\right), \quad L_z \to \infty, \tag{21}$$

where ξ_f is the decay correlation length, and λ_f is the wavelength of oscillations. Further, A_f is the amplitude and θ_f is the phase of the oscillatory decay. Earlier DFT studies of hard-sphere systems[6,31] have shown that the quantities ξ_f and λ_f are determined solely by the pair structure in the bulk system. That is true also for the real colloidal (silica) system at hand, which was demonstrated in Ref. 1. Another issue is the amplitude A_f and the phase θ_f of the oscillations, which is expected to depend on the nature of fluid-wall interaction.[6,31] Indeed, in Ref. 14 it was shown by GCMC simulations that variation of the surface potential of the walls strongly influences both, A_f and (θ_f). Here, we discuss our corresponding DFT results. We focus on the FMSA since we have seen in Sec. IV A that this approximation generally provides more satisfactory results as compared to MFA.

A comparison of FMSA and GCMC data for the solvation pressures in presence of differently charged surfaces and two bulk densities is given in Figs. 7 ($\rho_b^* = 0.200$) and 8 ($\rho_b^* = 0.440$). To facilitate the comparison, the curves are shifted along the y axis. We can see that upon changing the surface potential (of the walls) from $\psi_S = 0$ (uncharged walls) to $\psi_S = -40$ mV, the FMSA solvation pressure first decreases in the amplitude A_f, as does the curve predicted by GCMC. On the other hand, when ψ_S is further changed from -40 mV to -160 mV, the amplitude of the oscillations increases again, consistent with what is seen in the experiments and in the corresponding GCMC simulations.[14] From a theoretical point of view, the non-monotonic behavior of A_f reflects an underlying non-monotonicity of the fluid-wall potential, as it is discussed in detail in Ref. 14. We also observe from Figs. 7 and 8 that the phase shift of the solvation pressures decreases as ψ_S become more negative, reflecting that the fluid-wall potential effectively broadens. The narrow

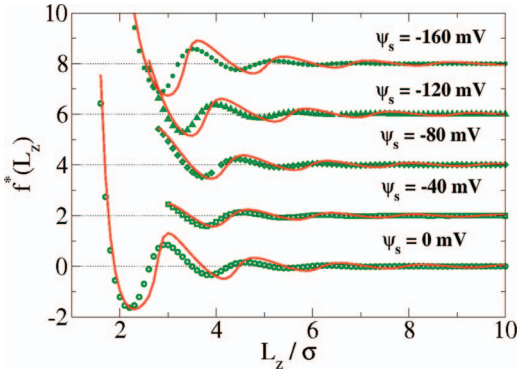

FIG. 7. Reduced solvation pressure f^* as a function of the wall separation L_z^* at different surface potential $\psi_S = 0, -40, -80, -120, -160$ mV . The corresponding bulk density is $\rho_b^* = 0.200$. For clarity the curves are shifted along the y axis.

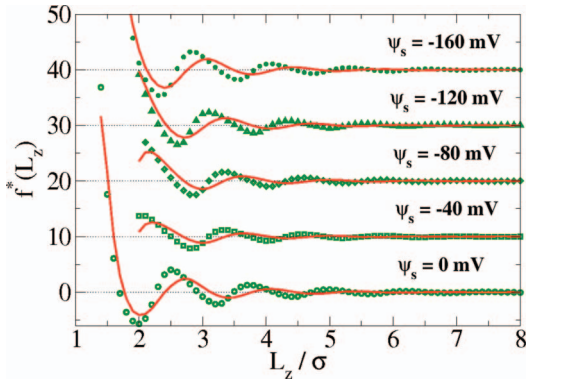

FIG. 8. The same as Fig. 6, but for $\rho_b^* = 0.440$.

potential at −40 mV hinders the entrance of colloidal particles into the slit pore particularly at small L_z^*. So far we have seen that FMSA is capable of predicting one main, experimentally detectable effect of surface modifications, that is, the increase of the amplitude A_f of the pressure oscillations upon increasing the absolute value of the surface charge. We now examine the behavior of the wavelength, λ_f, which is typically interpreted as a measure of the distance between the layers formed parallel to the confining surfaces. According to analytical predictions from DFT,[6,31] this wavelength is determined by the asymptotics of the bulk pair correlation function. Thus, it should be unaffected when one changes the surface charge, and thus, the fluid-wall potential.

To check this prediction in the context of the present DFT approach, we have fitted our results for the solvation pressure [see Figs. 7 and 8] according to the expression given by Eq. (21). Recalling that this expression holds only in the asymptotic limit, the fit has been started only from the first peak of the curve $f^*(L_z^*)$. Our results for the wavelength λ_f are summarized in Table I, where we have included data from GCMC as well as from corresponding DFT-MFA calculations. It is seen that both the FMSA and the MFA wavelengths remain essentially constant when ψ_S is changed, as one would expect based on earlier theoretical and simulation studies.[6,31] On a quantitative level, the DFT results overestimate the wavelength. Comparing the two approximations with the GCMC results, however, we find that the FMSA performs again much better than the MFA. For example, at the bulk density $\rho_b^* = 0.200$ (see left column in Table I), the FMSA value for λ_f has a relative error of about 6% as compared to the corresponding GCMC value. In MFA, on the other hand, the relative deviation is 17%. At the higher density $\rho_b^* = 0.440$ (see right column in Table I), these deviations increase to 9% and 32% in the case of FMSA and MFA, respectively.

TABLE I. Comparison of the wavelength obtained from fits for the cases with a bulk density $\rho_b = 0.200$ and $\rho_b = 0.440$.

	$\rho_b^* = 0.200$			$\rho_b^* = 0.440$		
ψ_s/mV	MC	FMSA	MFA	MC	FMSA	MFA
0	1.60	1.74	1.93	1.24	1.32	1.63
−40	1.65	1.71	1.90	1.24	1.34	1.60
−80	1.63	1.71	2.00	1.22	1.35	1.63
−120	1.60	1.73	1.83	1.22	1.33	1.63
−160	1.60	1.73	1.83	1.22	1.34	1.63

Nevertheless, both DFT approaches predict, in agreement with earlier studies,[1,14] that λ_f decreases upon increase of ρ_b^*. In the context of the MFA, which is a "structureless" approximation neglecting correlation effects, this variation of the wavelength seems somehow unexpected. We recall, however, that there is still the HS contribution to the free energy, which is treated in a highly sophisticated manner (i.e., by FMT) in both of our DFT approaches. We thus conclude, that the observed density dependence of the MFA-wavelength is essentially due to the HS interaction effects.

V. CONCLUSIONS

In this paper, we have used DFT and simulation methods to study charged colloidal suspensions confined in slit pores with uncharged and charged walls. The model employed here considers the interactions between macroions on an effective level, while the solvent particles are treated implicitly. Moreover, this model was previously used to study real silica colloidal systems, by means of simulations and integral equations methods.[1,12–15] Our present density functional approach involves the FMT functional to treat the short-ranged (hard core) contribution of the colloidal interactions, combined with the MFA and FMSA for the DLVO part. To evaluate the performance of these methods we have compared local density profiles and normal pressures to corresponding data from GCMC simulations. Exploring a broad range of densities and wall separations, it turns out that the FMSA yields overall more accurate results as compared to the MFA.

Specifically, considering first uncharged walls, we have found that the FMSA provides quite accurate density profiles for bulk densities in the range $\rho_b^* \lesssim 0.200$. A similar conclusion was reached in a recent DFT study of Louis *et al.*,[11] who used the same FMSA approach to study Yukawa fluids (with repulsive or attractive Yukawa tail) at somewhat smaller interaction strength. Fixing the bulk density to $\rho_b^* = 0.191$, they also found satisfactory agreement between their DFT and simulation results. An important difference between the model used here and that in Ref. 11 is that their screening parameter does not depend on the density. Nevertheless, the conclusions are very similar.

At higher density, our DFT results based on the FMSA show that this theory still yields a good description of the local structure at some specific wall separations. These wall separations correspond to relative minima of the normal pressure (as a function of L_z) in the range of small wall separations, where the pressure oscillations become pronounced. However, comparing the entire curves $P_{zz}(L_z)$ in FMSA with the simulation results, we find a shift towards somewhat larger wall separations. This shift is related to the fact that the FMSA is characterized by a delay in predicting formation of a new layer when the wall separation is increased from low values (at fixed ρ_b^*). Interestingly, the shift is more pronounced at large wall separations, where the structure in the confined system should be dominated by fluid-fluid interactions. This

suggests a general difficulty of the FMSA to predict correctly the *bulk* pair correlation function at high densities. A further hint for inaccuracies of the FMSA in dense systems is the fact that the bulk pressure suggested from the FMSA curve $P_{zz}(L_z)$ at large L_z differs significantly from the corresponding GCMC result. Nevertheless, the FMSA still provides a valuable description on a qualitative level at the most of the wall separations in the sense that the number of layers in the system are described correctly. The MFA, on the other hand, yields reasonable results only at very low densities. At larger bulk densities and large wall separations, MFA is not even able to predict the structure qualitatively.

In the last part of the paper, we have studied our model fluid in presence of charged walls, using the fluid-wall potential developed in Ref. 14. Our goal was to investigate the influence of charged surfaces (with varying surface charges) on the oscillatory decay of the solvation pressure. Our present DFT-FMSA results confirm the observation previously made in the GCMC simulations and in experiments,[14] that the amplitude A_f and the phase shift depend on the fluid-wall interaction (i.e., the surface charge). On the other hand, our results also confirm that the wavelength does not depend on the external potentials, which is consistent with previous theoretical studies[31,32] as well as with simulations/experiments.[14] Moreover, the FMSA predictions for the wavelength are quite accurate from a quantitative point of view.

Taken altogether, the results of the present DFT study show that combining the FMT approach with a sophisticated perturbative treatment of the long-range, screened Coulomb (here: DLVO) interactions yields a valuable tool to describe inhomogeneous charged colloidal suspensions at not too high densities and coupling strength. These general findings are consistent with those in Ref. 11 where both repulsive and attractive Yukawa fluids were considered. Moreover, the breakdown of the simpler MFA suggests that it is very important to use approximations which do not neglect the pair correlations of the fluid. Based on these insights, it is now tempting to use the DFT-FMSA approach also for more complicated systems of confined charged colloids where, e.g., disorder plays a role. Work in this direction is in progress.

ACKNOWLEDGMENTS

A.G. would like to thank G. Rosenthal for fruitful discussions on the numerical implementation of FMT. Furthermore, he gratefully acknowledges financial support from the JAE-Predoc program. A.G. and N.G.A. acknowledge financial support from the Dirección General de Investigación Científica y Técnica under Grant No. FIS2010-15502, and from the Dirección General de Universidades e Investigación de la Comunidad de Madrid under Grant No. S2009/ESP-1691 and Program MODELICO-CM. S.G. and S.H.L.K. would like to thank the German Research Foundation (DFG) for financial support within the Collaborative Research Center (CRC) 951 "Hybrid Inorganic/organic systems for Optoelectronics" and the International Graduate School (IRTG) 1524 "Self-assembled soft-matter nanostructures at interfaces."

[1] S. H. L. Klapp, Y. Zeng, D. Qu, and R. v. Klitzing, Phys. Rev. Lett. **100**, 118303 (2008).
[2] Y. Rosenfeld, Phys. Rev. Lett. **63**, 980 (1989).
[3] R. Roth, J. Phys.: Condens. Matter **22**, 063102 (2010).
[4] J. P. Hansen and I. R. McDonald, *Theory of Simple Liquids* (Academic, Amsterdam, 2006).
[5] Y. Rosenfeld, J. Chem. Phys. **98**, 8126 (1993).
[6] R. Roth, R. Evans, and S. Dietrich, Phys. Rev. E **62**, 5360 (2000).
[7] M. Schmidt, A. Fortini, and M. Dijkstra, J. Phys.: Condens. Matter **48**, s3411 (2003).
[8] E. Lomba, M. Alvarez, L. L. Lee, and N. G. Almarza, J. Chem. Phys. **104**, 4180 (1996).
[9] E. Kierlik and M. L. Rosinberg, Phys. Rev. A **44**, 5025 (1991).
[10] Y. Tang and J. Wu, Phys. Rev. E **70**, 011201 (2004).
[11] S. Karanikas, J. Dzubiella, A. Moncho-Jordá, and A. A. Louis, J. Chem. Phys. **128**, 204704 (2008).
[12] S. H. L. Klapp, S. Grandner, Y. Zeng, D. Qu, and R. v. Klitzing, J. Phys.: Condens. Matter **20**, 494232 (2008).
[13] S. H. L. Klapp and S. Grandner, J. Chem. Phys. **129**, 244703 (2008).
[14] S. Grandner, Y. Zeng, R. v. Klitzing, and S. H. L. Klapp, J. Chem. Phys. **131**, 154702 (2009).
[15] S. H. L. Klapp, D. Qu, and R. v. Klitzing, J. Phys. Chem. B **111**, 1296 (2007).
[16] E. J. W. Verwey and J. T. G. Overbeek, *Theory of Stability of Lyphobic Colloids* (Elsevier, Amsterdam, 1948).
[17] J. A. Barker and D. Henderson, J. Chem. Phys. **47**, 2856 (1967).
[18] J. A. Barker and D. Henderson, J. Chem. Phys. **47**, 4714 (1967).
[19] S. Bhattacharjee, M. Elimelech, and M. Borkovec, Croat. Chem. Acta **71**, 883 (1998).
[20] H.-J. Butt, K. Graf, and M. Kappl, *Physics and Chemistry of Interfaces* (Wiley VCH, Weinheim, 2006).
[21] R. Roth, R. Evans, A. Lang, and G. Kahl, J. Phys.: Condens. Matter **14**, 12063 (2002).
[22] Y. Tang, J. Chem. Phys. **118**, 4140 (2003).
[23] E. Waisman, Mol. Phys. **25**, 45 (1972).
[24] L. G. MacDowell, M. Muller, and D. V. K. Binder, J. Chem. Phys. **113**, 419 (2000).
[25] P. Hohenberg and W. Kohn, Phys. Rev. **136**, B864 (1964).
[26] R. Evans, Adv. Phys. **28**, 143 (1979).
[27] R. Evans and M. B. Marconi, J. Chem. Phys. **86**, 7138 (1987).
[28] B. Widom, J. Chem. Phys. **39**, 2802 (1963).
[29] D. Frenkel and B. Smit, *Understanding Molecular Simulation* (Academic, London, 1996).
[30] M. Schoen and S. H. L. Klapp, in *Reviews in Computational Chemistry*, edited by K. B. Lipkowitz and T. R. Cundari (Wiley, New Jersey, 2007).
[31] C. Grodon, M. Dijkstra, R. Evans, and R. Roth, Mol. Phys. **103**, 3009 (2005).
[32] R. Evans, J. R. Henderson, D. C. Hoyle, A. O. Parry, and Z. A. Sabeur, Mol. Phys. **80**, 755 (1993).